Supplemental Material: A low-cost $PM_{2.5}$ monitor for wildland fire smoke

Scott Kelleher[1], Casey Quinn[2] Daniel Miller-Lionberg[1], and John Volckens[1]

[1]Department of Mechanical Engineering, Colorado State University, Fort Collins, USA

[2]Department of Environmental and Radiological Health Sciences, Colorado State University, Fort Collins, USA

Correspondence to: John Volckens (john.volckens@colostate.edu)

Table S1. Components added to UPAS to form the OAS

Component	Manufacturer	Part number	Cost
Polycrystalline Solar Cell	Banggood	991137	3@$5
Voltage Regulator	ProDCtoDC	90462	$5
Microcontroller/SMS Module	Particle	Electron 3G	$59
MicroSD card logger	Molex	5031821852	$7
Battery (2800 mAh)	Anker	7OSMS5-28N	3@$14
Temp, Pressure, RH sensor	Bosch Sensortec	BME280	$10
Current/Voltage Sensor	Texas Instruments	INA219	$10
Low-cost PM Sensor	Sharp	GP2Y1010AU0F	$8
Sharp Sensor adapter	DFRobot	DFR0280	$4
Weatherproof enclosure	Pelican	1020 micro	$14
Magnets	KJ Magnetics	BX08H1	7@1.3

Table S2 lists all input variables used in the simulation design. The amount of daily solar irradiance available (*S*), is the simulation's only Monte Carlo sampled input.

Table S2. Power design model variables

Variable	Term	Input (units)	Data Source
R	Rated Battery Capacity	10.78 (Watt-hours)	Determined Empirically
E	Solar Circuit Efficiency	7.50%	Determined Empirically
N	Battery Quantity	5 (unit less)	Determined Empirically
T	Temperature	Monthly mean of daily low temperatures(ºC)	CSU Christman Weather Station
P	OAS Daily Power Consumption	16.8 (Watt-hours)	Determined Empirically
S	Solar Irradiance Available	Monte Carlo sampled daily value (watt-hrs.)	
V	Useable Battery Capacity Percentage	0.85 (fractional percentage)	Determined Empirically
C	Battery Capacity Temperature Correction	Equation 2 (unitless)	

Useable battery capacity percentage (V) was determined to be 85% based on OAS circuit cutoff voltages. Fully charged battery capacity B_0, where the subscript refers to day '0', can be expressed using Eq. (1);

$$B_0 = R * N * C_i * \mathrm{V} \qquad (1),$$

where R is rated battery capacity, N is battery quantity, C_i is the capacity correction from temperature (for month i), and V is useable battery capacity percentage. The Li-ion battery capacity correction factor, C, as a function of month, i, for an 18650b battery type, is described in Eq. (2);

$$C_i = (-0.0097T_i^2 + 0.8061T_i + 90)/100 \qquad (2),$$

where T(ºC) is the mean low temperature across a given month, i . Eq. (3) is used to calculate the runtime (in days) for each of the 1000 sampling missions each month;

$$Runtime\ (days) = \sum_{d=1}^{14} \begin{Bmatrix} 0\ if\ (B_{d-1} - P + S * E) > 0 \\ 1\ if\ (B_{d-1} - P + S * E) < 0 \end{Bmatrix} \qquad (3),$$

where B is battery capacity at the conclusion of day d, P is daily OAS power consumption, S is available solar irradiance and E is solar energy conversion efficiency.

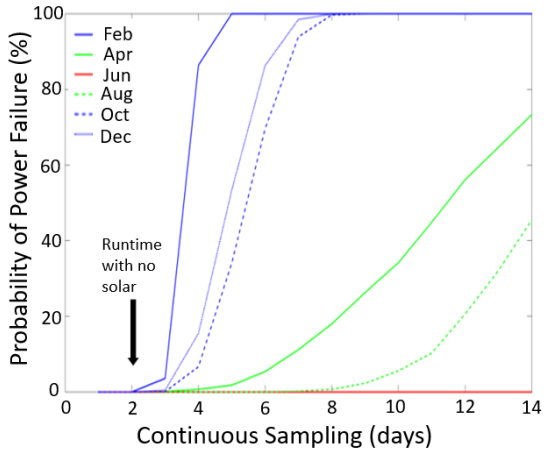

Figure S1. Monte Carlo simulation results showing OAS power failure probability for every other month of the year. Axes define number of continuous sampling days and probability of power failure. Colors represent selected months spanning four seasons.

Particle collection efficiency of the Tisch PTFE filters (Figure S2) was evaluated in an aerosol chamber; wood smoke was used to simulate prescribed fire aerosol. A scanning mobility particle sizer (SMPS, model 3082, TSI Inc., Shoreview, MN) was used to count particles in 110 discrete size ranges from 19 to 1000 nm. A set of repeated measures was made with a Tisch PTFE filter inline and then removed (alternating the order between sets) for four test filters, three sets per filter. Additional chamber air (1.4 L/min) was metered through the filter to make up the

Deleted: f

difference between the intended OAS flowrate (2 L/min) and the flow into the SMPS, which was nominally 0.6 L/min.

Filter collection efficiency for each particle size range was determined using Eq. (6);

$$filter\ collection\ efficiency_i = \eta_i = 1 - \frac{N_{i,on}}{N_{i,off}} \quad (6),$$

where $N_{i,on}$ is the particle count measured by the SMPS with filter on, $N_{i,off}$ is the particle count measured by the SMPS with filter off and i represents the midpoint of each particle size range. Mass collection efficiency of the Tisch filter was estimated for prescribed fire aerosol using an aerosol size distribution specific to wildland fire. This distribution was modeled from a lognormal distribution having a count median diameter (CMD) of 70 nm and geometric standard deviation (σ_g) of 1.7 (Sakamoto et al., 2016). The mass of a single particle in each particle size range ($m_{p,i}$) was calculated using Eq. (7),

Deleted: modeled

$$m_{p,i} = \frac{\pi}{6} d_i^3\, \rho \quad (7),$$

where d_i is the median particle diameter for each size range, i, and ρ is particle density. The mass in each particle size range (M_i) can be calculated using Eq. (8),

$$M_i = N_i\, m_{p,i} \quad (8),$$

where N_i is the number of particles present in size range *i*. The mass collection efficiency of the filter is determined by the ratio of particulate mass collected by the filter to total particulate mass. Percent mass collection efficiency is calculated using Eq. (9):

$$mass\ collection\ efficiency = \frac{\sum_{i=1}^{n} \eta_i M_i}{\sum_{i=1}^{n} M_i} * 100 \quad (9),$$

where the numerator on the right hand side represents the particulate mass collected by the Tisch filter (determined experimentally) summed up over n size ranges and the denominator is the summation of particulate mass across equivalent size ranges for a hypothetical biomass burning aerosol (Sakamoto et al., 2016). Filter collection efficiency has been found to increase with filter loading (Soo et al., 2016). The mass collection efficiency of a clean Tisch filter was considered to be constant when correcting prescribed fire filter mass accumulated for collection efficiency.

The average collection efficiency is depicted in Figure S2 by a black line; grey shading represents ± 1 standard deviation. The red plot represents a hypothetical aerosol mass distribution produced by prescribed fire (derived from (Sakamoto et al., 2016)).

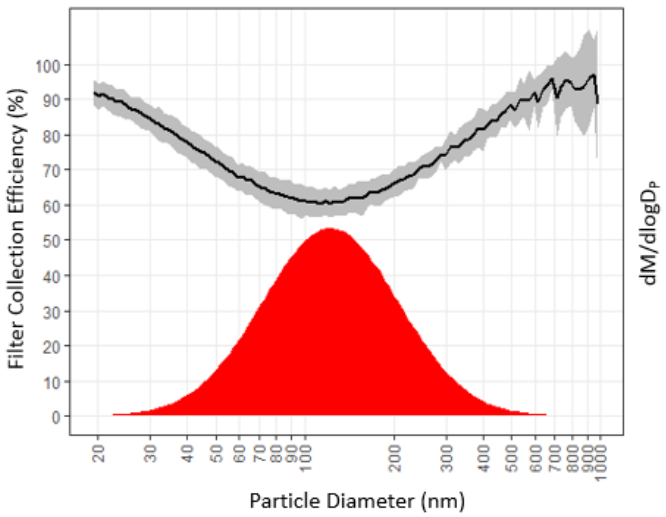

Figure S2. Collection efficiency of 37mm Tisch PTFE filters (2L/min flow) with respect to particle mobility diameter and mass distribution of particles (red). Primary vertical axis represents filter collection efficiency; secondary vertical axis represents particle size distributions (by mass). Horizontal axis is particle size**.**

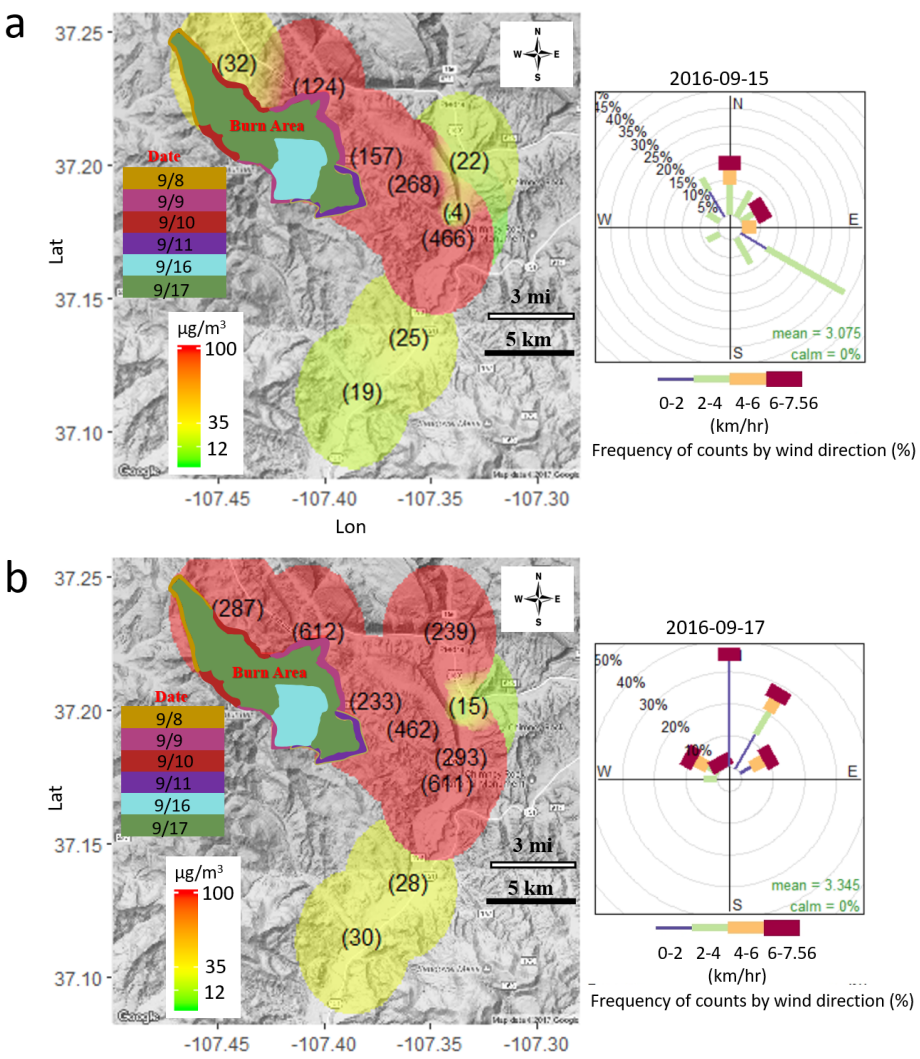

Figure S3. Maps illustrating spatial concentration gradients and the temporal evolution of fire emissions for Sept 15th, and 17th, 2016. Numbers indicate 24-hour average mass concentration at each sampling site (e.g. (57) refers to a mass concentration of 57 µg/m^3).

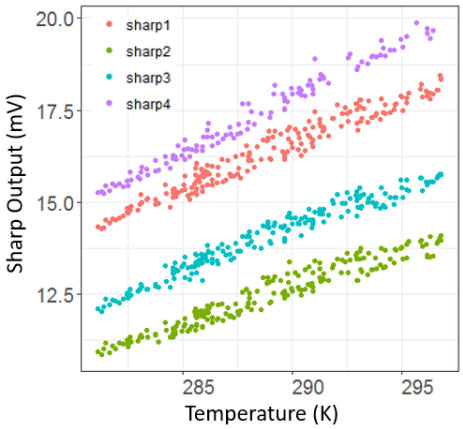

Figure S4. Sharp sensor (GP2Y1023AU0F) output correlation with ambient temperature.

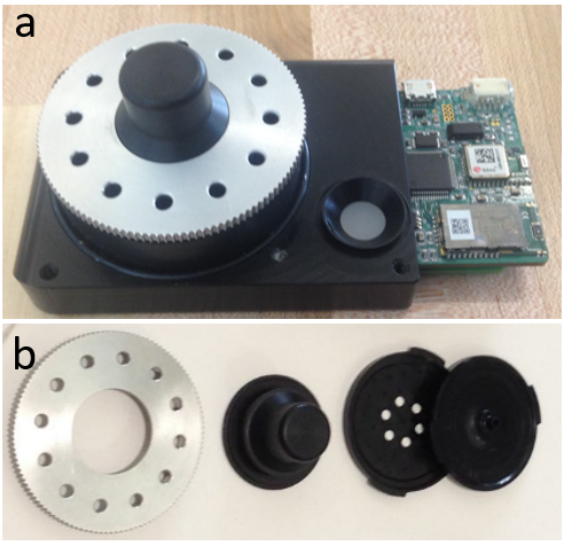

Figure S5. a) UPAS sampler with threaded aluminium inlet in place b) threaded aluminium inlet, size-selective cyclone, and filter cartridge.

The run performance of each OAS on each prescribed fire deployment is shown in Fig. S6. Any OAS that operated without issue is shown in green, OAS that experienced a power failure or other technical failure are shown in red and orange, respectively. Power failure was defined as sampling for less than the 24-hour goal due to depletion of battery power. Other common failure modes were if average OAS flow rate was not within 12.5% of specified flow rate (2 L/min) or if the instrument failed to turn on at the specified time. Power consumed by the OAS is strongly dependent on filter loading, which is a function of the sampled aerosol mass concentration. High filter loadings create greater than normal pressure drops across the OAS filter, forcing the pumps to work harder to maintain flow rate. As a result, the OAS consumes more power, which decreases runtime. Eleven of twelve OAS successfully completed the 24-hour sampling period on 9/15/2016. Five OAS fully completed the 24-hour sampling period on 9/18/2016 while 5 experienced power failure. Depleted from 4 previous 24-hour sampling periods and the high $PM_{2.5}$ concentrations experienced on 9/17/2016, 9/18/2015 saw 5 of the 12 samplers fail due to lack of power.

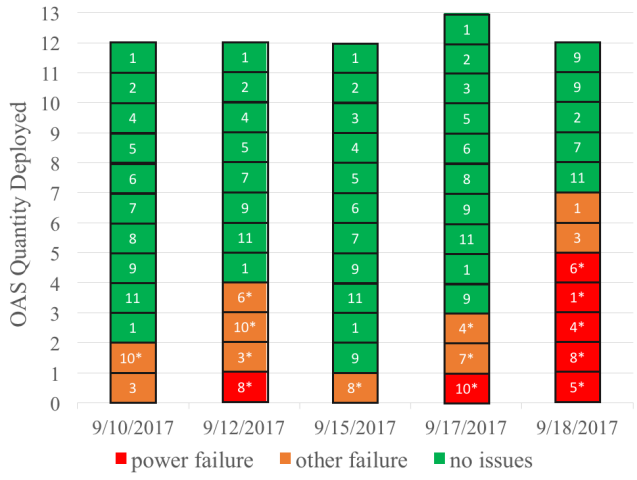

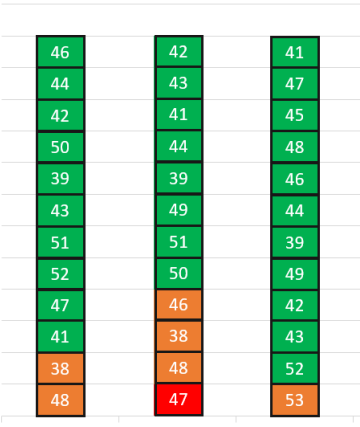

Figure S6. The operational status of each OAS at the conclusion of each sampling day. Colors represent failure mode; numbers in each rectangle represent OAS sampling locations as identified in Figure 3. Asterisks represent high-$PM_{2.5}$ concentration events (leading to premature OAS power failure) that were extrapolated out to 24-hr time-weighted averages for inclusion into Figures 7 and S3. To note, these failure events were not included in Figure 8, which compared valid OAS measurements against reference $PM_{2.5}$ measurements.

Deleted: ;

Deleted: F

Deleted: or

Deleted:

Deleted: identification number

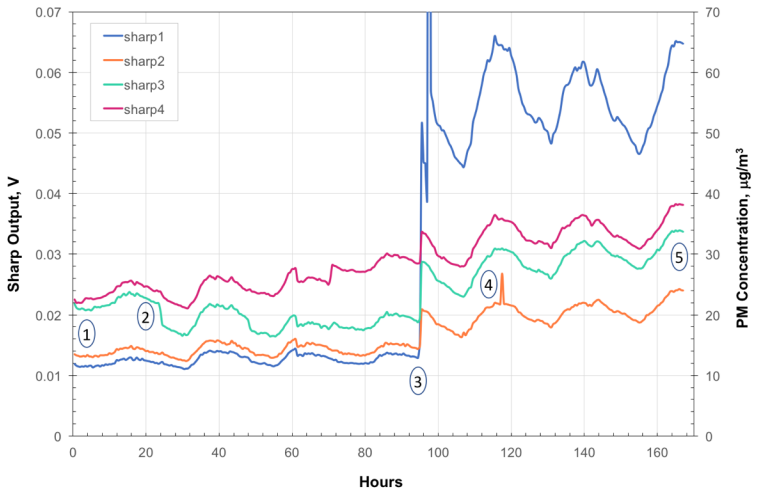

Figure S7. Time series data for Sharp sensors co-located outdoors in a shaded enclosure for 170 hours (~7 days). For this deployment, one millivolt of sensor output corresponds to approximately 1 µg/m^3 of $PM_{2.5}$ concentration. Selected 'events' annotated 1-5 are described in the text below and serve as examples of why sensor drift rendered the Sharp data unreliable in the field.

1. Hour 1: At the start of the sampling period, the four Sharp sensors are offset from each other by nearly 100% from lowest to highest, reporting PM concentrations that vary from 12 to 22 µg/m^3. The lack of precision among co-located sensors is common.

2. Hour 20: The close agreement between Sharp sensors #3 and #4 begins to diverge. Based on examination of all sensor traces, Sharp #3 appears to be experiencing drift relative to the other three devices.

3. Hour 95: All four Sharp sensors experience a sudden rise in output voltage, which produces a dramatic change in both their absolute readings and relative offsets. This effect appears to persist from this point forward. Note how far Sharp 1 is now offset from the other three Sharp sensors.

4. Hour 116: Sharp #2 experiences a phantom spike not seen by the other three sensors (all sensors were co-located in a single box).

5. At the end of the sampling period (hour 170), the four Sharp sensors now report values that are offset from 25 to 65 µg/m^3 from each other, a factor of four increase in the difference from lowest to highest reading relative to the start of the sampling period.